Surface & Coatings Technology 253 (2014) 68–75

Contents lists available at ScienceDirect

Surface & Coatings Technology

journal homepage: www.elsevier.com/locate/surfcoat

Effect study and application to improve high cycle fatigue resistance of TC11 titanium alloy by laser shock peening with multiple impacts

Xiangfan Nie [a,*], Weifeng He [a], Shunlai Zang [b], Xuede Wang [a], Jie Zhao [b]

[a] Science and Technology on Plasma Dynamics Lab., Air Force Engineering University, Xi'an, Shaanxi 710038, China
[b] School of Mechanical Engineering, Xi'an Jiaotong University, Xi'an, Shaanxi 710049, China

ARTICLE INFO

Article history:
Received 16 December 2013
Accepted in revised form 15 May 2014
Available online 21 May 2014

Keywords:
Laser shock peening
TC11 titanium alloy
Nanostructure
High cycle fatigue
Strengthening mechanism

ABSTRACT

Laser shock peening (LSP) is an effective surface treatment for improving fatigue resistance of metallic materials, in which high-amplitude beneficial residual stresses and structure changes can be produced. In aero-engines, the compressor blade made of TC11 titanium alloy was prone to result in high cycle fatigue (HCF) failure. The aim of this paper was to utilize LSP with befitting parameters to improve the HCF performance of TC11 titanium alloy. Firstly, the microstructure and mechanical properties of TC11 titanium alloy with different LSP impacts were observed and measured via transmission electron microscope (TEM), residual stress tester and microhardness tester. High-density dislocations and nanostructure were observed in the surface layer. High-amplitude compressive residual stresses were induced and microhardness was remarkably improved. According to the effects, a set of LSP parameters with three LSP impacts was confirmed and applied on standard vibration specimens. Vibration fatigue tests were conducted to validate the strengthening effect on HCF strength. The fracture mechanism was analyzed by fracture analysis. The strengthening mechanism of LSP was indicated by establishing the relationship between fatigue characteristics and effects on residual stress and microstructural changes.

1. Introduction

With the rapid development of military aircraft, high performance aero-engines have brought forward a higher property required for materials and components, especially aero-engine with a thrust-weight ratio greater than 10. The new materials with better performance and new material processing technologies are needed to be adjusted to the more terrible working environment in aero-engine. Because a new material will be invented in a long period, the strengthening technologies are becoming more and more practical. As to engineering components, the maximal tensile stress always locates at the surface, where the fatigue crack is prone to initiate. In order to improve the fatigue strength, the surface treatment technologies, such as deep rolling (DR), shot peening (SP) and LSP, have been studied and successfully applied to some kinds of metallic materials. They can produce microstructural changes, such as dislocations and twins, and induce compressive residual stresses [1–3].

Compared with conventional SP, LSP is very effective in improving metallic material properties [4], such as resistance of fatigue [5–7], corrosion [8,9] and wear [10]. In the past, LSP has been applied in many alloys and proved to be effective in improving HCF strength. After LSP, the fatigue crack initiation can be retarded and growth rate can be reduced [11,12]. When foreign object damage (FOD) was occurred in fan/compressor blades, the fatigue crack will be initiated and extends quickly under working stress. LSP was adopted to improve the HCF performance and FOD damage tolerance and the feasibility has been proved [13]. GE, P.W, MIC and LSPT have successfully applied this technology in engines of F101, F110, F404 and F119.

In aero-engines, the compressor blade is always made of titanium alloy, because the mechanical performance is so attractive with a high specific strength. Some researches about the effects of LSP in titanium alloys have been done and reported. Ikuya Watanabe et al. [14] have utilized LSP to improve the tensile property of cast titanium. C. Cellard et al. [15] have studied on the influence of different LSP parameters for Ti-17 titanium alloy via the aspects of residual stress, work-hardening, surface topography and curvature. Owing to the fracture problem of titanium alloy compressor blades, there were also some works about LSP application to enhance the HCF performance. Ruschau et al. [16,17] examined and compared the fatigue nucleation and crack growth rate (FCGR) characteristics of laser-peened Ti–6Al–4 V with an unprocessed material. They demonstrated that the FCGR resistance of LSP processed samples was significantly improved at lower stress ratio (R) but diminished at high. Zhang et al. [18] addressed the effects of multiple laser peening and laser peening intensity on the residual stress, microhardness and three-point bending fatigue performance of Ti–6Al–4 V alloy. It is found that the fatigue life of laser-peened specimen increases with the number of overlapped laser spot, reaches a local maximum with three overlapped laser spots and then decreases. E. Maawad et al. [19] indicated that the HCF performance of α Ti-alloy Ti–2.5Cu and β Ti-

* Corresponding author. Tel.: +86 029 84787537.
E-mail address: skingkgd@163.com (X. Nie).

http://dx.doi.org/10.1016/j.surfcoat.2014.05.015
0257-8972/

alloy TIMETAL LCB was more improved by applying laser shock peening without coating (LPwC) than by applying conventional shot peening. But it is contrary for the α + β Ti-alloy TIMETAL 54M.

The above studies addressed the effects of LSP on HCF performance, in which compressive residual stress was regarded to be the primary cause for HCF strength improvement. And the beneficial contribution of structural changes was ignored. Nikitin [20] and Altenberger [21] discussed the effects of structural changes on HCF behavior in Ti–6Al–4 V. They found that structural changes also played a positive role for HCF performance, especially at elevated temperature. In addition, a nanostructure layer was observed in TC6 and TC17 titanium alloy surface [22,23]. The nanostructure will be the dominated strengthening factor for HCF performance in a working condition (elevated temperature and cycle loading) with residual stress relaxed. So we focused on the formation and evolvement rule of a nanostructure in this paper.

In order to resolve the HCF fracture problem of TC11 titanium alloy compressor blades, LSP is needed to be applied to improve the HCF resistance. In this study, the effects of LSP in TC11 titanium alloy were studied in detail. In order to discuss the influence rule of LSP impact, the TC11 titanium alloy samples were processed with different LSP impacts. The microstructure and mechanical properties were studied by the methods of TEM observation, residual stress test and microhardness test respectively. According to the influence rule of LSP impact, the most appropriate LSP impact was chosen and applied on the vibration specimens. The vibration fatigue test was conducted to validate the strengthening effect of LSP on HCF performance. And the fracture mechanism was analyzed by a scanning electron microscope (SEM). Considering the LSP effects on microstructure and mechanical property synthetically, the strengthening mechanism for high cycle fatigue performance was indicated.

2. Experiment details

2.1. Materials and components

The TC11 titanium alloy is one of most widely used Ti–Al–Mo–Zr–Si series titanium alloys in the China aviation field, and is also named as Ti–6.5Al–1.5Zr–3.5Mo–0.3Si. The chemical composition of this alloy (in wt.%) is given in Table 1 [24]. This alloy used in the present study was produced and machined into vibration fatigue specimens by the Li-Ming Aero-Engine Company of China Aviation Industry. TC11 titanium alloy is a kind of α + β type heat-resisting titanium alloy with an outstanding combination property. It is mainly used to manufacture compressor blades and disks in aero-engines. The heat treatment was double annealing, 950–980 °C/2 h air cooled and 530/6 h air cooled. The material properties of this alloy at room temperature are listed in Table 2.

Fig. 1 shows the optical micrograph of TC11 titanium alloy. It describes that this alloy is composed of 60% (by volume) primary hexagonal close-packed (hcp) alpha phase and 40% lamellar transformed body-centered cubic (bcc) beta phase. The α-grain is equiaxial and the β-grain is acicular. The average size of α-grains is ~8 μm. A diagrammatic sketch of the samples for microstructure observation and mechanical properties measurement is shown in Fig. 2.

2.2. Principle and experimental procedure of LSP

LSP is an innovative surface treatment technique utilizing a laser pulse with short pulse width (ns) and high power density (GW/cm^2) to strike on the target surface. In the LSP process as shown in Fig. 3, the laser-peened target is covered by two different layers, namely an opaque ablating layer and a transparent confining layer. Firstly laser pulse passes through the transparent confining medium and strikes on the ablating layer. Then the laser pulse is absorbed by the ablating layer which immediately vaporizes and forms plasma with high temperature and pressure. The expanding of the plasma detonation wave leads to the formation of shock wave which propagates into the target with an intensity of several GPa. If the pressure of shock wave is greater than the dynamic field strength of the target material, plastic deformation will be generated with compressive residual stresses and structural changes in the surface layer.

During the LSP process in this study, the square samples were mounted on a five-coordinate robot arm which was controlled in the x–y direction to implement the designed laser-shocked paths, shown in Fig. 2. The confining layer and ablating layer were floating water (1–2 mm thick) and Al foil (0.1 mm thick) respectively. The laser pulse with a wavelength of 1064 nm and a pulse of 20 ns was generated by a Nd:YAG laser designed by ourselves (SGR-EXTRA/25 J). The laser power density was 4.24 GW/cm^2 which was confirmed by previous experiments [23]. In order to discuss the influence rule of LSP impact and confirm the best LSP impact, the TC11 titanium alloy samples were treated with different impacts (0/1/3/5/10). The other detailed LSP parameters are the following: laser pulse with a wavelength of 1064 nm, a pulse energy of 6 J, a spot diameter of 3 mm, a lapping rate of 60% and a repetition-rate of 1 Hz.

Table 1
Chemical composition of titanium alloy.

Composition	Al	Mo	Zr	Si	Fe	Ti
Percent (wt.%)	5.8–7.0	2.8–3.8	0.8–2.0	0.15–0.40	0.2–0.7	Bal

Table 2
Static tensile properties of TC11titanium alloy at room temperature.

Yield strength $\sigma_{0.2}$/MPa	930
Ultimate tensile strength σ_b/MPa	1030
Elongation rate δ/%	9
Contraction rate ψ/%	30

3. Microstructural observations

3.1. TEM observations

Under the shock wave induced by LSP, severe plastic deformation is generated in the surface layer. Kinds of microstructural changes can be formed, for instance dislocations, twins and grain refinement. The

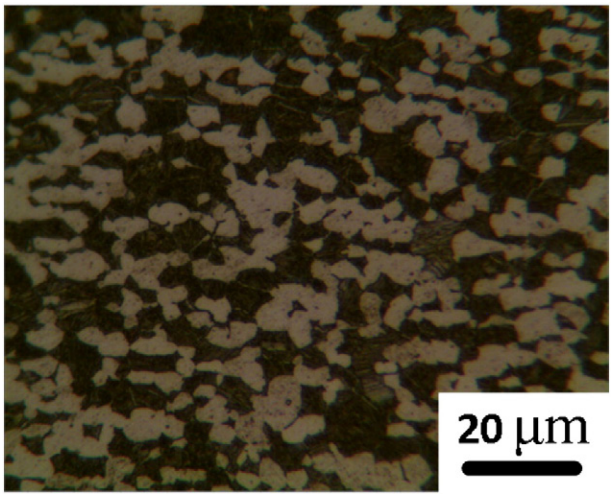

Fig. 1. Optical micrograph of TC11 titanium alloy (etched for ~12 s in a solution of five parts 70% HNO_3 and ninety-five parts of absolute alcohol).

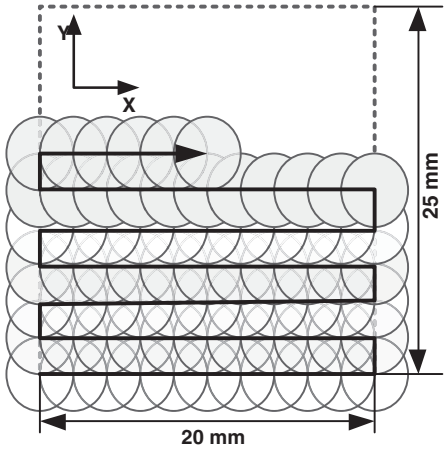

Fig. 2. Dimensions and LSP processed area of samples for microstructure observation and mechanical property tests (the dashed region is the LSP processed area with a 25 mm × 20 mm dimension on one side).

microstructure in the material surface without and with LSP was observed by TEM-3010 transmission electron microscope. Fig. 4 shows the TEM micrographs and diffraction patterns of the TC11 titanium alloy surface with different LSP impacts. And different microstructural characteristics have been observed.

Fig. 4(a) shows the original typical features of TC11 titanium alloy. The alloy is a double-phase titanium alloy and composed of two phases: α phase and β phase. The equiaxial phase is the α phase, and the β phase is acicular. Phase boundary can be easily authenticated, and the size of these phases is very great, about 10 μm in the largest direction. High density dislocations and dislocation walls are exhibited in Fig. 4(b) with one LSP impact and the diffraction pattern is anomalistic. The size of the dislocation wall is ~1 μm. Lots of nanocrystals are generated with three LSP impacts and the average grain size is ~70 nm in Fig. 4(c). The diffraction pattern appears as a diffraction ring with a random orientation. It indicates that the original grains are refined into nanocrystals via dislocations slipping. The nanostructure in the surface layer is correlating with the results of Ti–6Al–4 V, TC6 and TC17 [20–23]. It demonstrates that the nano-crystalline phenomenon in titanium alloys is common and can be realized by multiple LSP impacts. When the LSP impact increases further, the average grain size gets smaller, about 40 nm with five or ten LSP impacts in Fig. 4(d) and (e). The grain orientation of the nanocrystals becomes more random and uniform. But the average grain sizes with five and ten LSP impacts are almost same. It illustrates that increasing LSP impact can produce smaller grains, whereas the size will get invariable with five LSP impacts. The evolvement rule of the nanostructure in TC11 titanium alloy is correlated with that in the titanium alloys of TC6 and TC17 [23,25]. The evolvement rule and grain refinement mechanism are similar in (α + β) Ti-alloys after LSP.

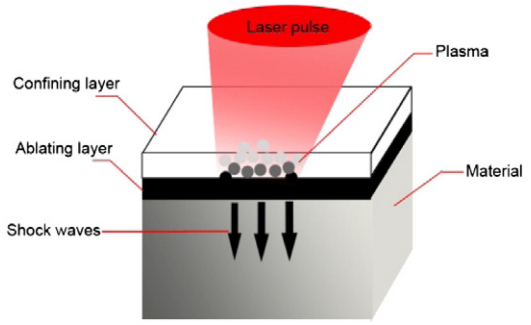

Fig. 3. Schematic principle of laser shock peening. The confining layer and ablating layer are water and Al foil, respectively.

3.2. Discussion on grain refinement

As for the generated nanocrystals, the evolvement mechanism of surface nanocrystallization [26] in TC11 titanium alloy is similar to the one caused by severe plastic deformation methods, such as shot peening and surface mechanical attrition treatment [27–30]. We have discovered the similar phenomena in TC6 titanium alloy, and preliminarily discussed the refinement mechanism [22]. J. Z. Lu et al. [31,32] have investigated the grain refinement mechanism in LY2 and ANSI 304 stainless steel by multiple LSP impacts. As for LSP, shock wave with high pressure is the special feature. M. A. Meyers has put forward the homogeneous nucleation theory [33,34] about the dislocation formation. The dislocations are generated on the wave front and driven to slip. Dislocations slip and accumulate at some place in the grains. And then high density dislocations and dislocation walls are formed in succession. The result in Fig. 4 is well consistent with the results of the researches of J. Z. Lu, Clauer, Zhang and Peyre [31,35–37], who have revealed that the dislocation density increases significantly after LSP. As a result of reflection, refraction and transmission of the shock wave on the grain surface, the approximately uniaxial load of shock wave is evolved into multidirectional loads which stimulate the locomotion of the dislocations. The dislocations ultimately transform into dislocation walls, sub-boundaries and grain boundaries. Latter plastic deformation induced by latter LSP impacts results in rearranging the resultant dislocation to form dislocation networks and nanocrystals. With more impacts, the refined grains are refined further until the refined grains get stable. When the grains are not able to be refined, the shock wave induced by latter LSP impacts can make the refined grains turn and obtain different grain orientations.

In conclusion, the LSP treatment with 3 LSP impacts can realize the surface nanocrystallization of this alloy. Increasing LSP impact can accelerate the grain refinement further and get more nanocrystals with smaller size and more uniform grain orientation.

4. Residual stress distribution

Severe plastic deformation was induced by LSP in the material surface. Much lattice distortion such as dislocations and new grain boundaries (shown in Fig. 4) were generated. Besides, high-amplitude compressive residual stresses are induced in the surface layer, which are very beneficial for the fatigue resistance. The residual stress was measured by the Proto-LXRD X-ray diffractometer with $\sin^2\psi$-method. The X-ray beam diameter was 2 mm and the diffracted Cu-kα characteristic X-ray from a Ti {213} plane was detected with a diffraction angle (2θ) of 137–145°. The sample was removed layer by layer via electrolytic polishing with a corrosion rate of 0.2–0.5 μm/s each 1 cm^2 (polishing solution: 95% saturated NH_4Cl solution + 5% $C_3H_8O_3$ solution).

The residual stress distribution curves on the cross-section with different LSP impacts are depicted in Fig. 5. It shows that LSP introduces great compressive residual stresses in TC11 titanium alloy and the maximal compressive residual stress is at the material surface. There is a machining stress of ~−30 MPa at the surface with a shallow affected layer before LSP. The surface residual stress is −541.6 MPa for 1 impact, −589.2 MPa for 3 impacts, −610.3 MPa for 5 impacts and −632.5 MPa for 10 impacts. The increased amplitude of compressive residual stress for each latter impact decreases with the LSP impact. It demonstrates that increasing LSP impact can improve the compressive residual stress restrictedly. It may be attributed to the plastic deformation limit of the material in the surface. It means that plastic deformation can't continue to be generated even with more LSP impacts. When the anterior impact improves the strength of the material in the surface, the latter impact is hard to generate plastic deformation in the same degree. The strengthening effect of the anterior impact inhibits the further plastic deformation in the latter impact to some extent.

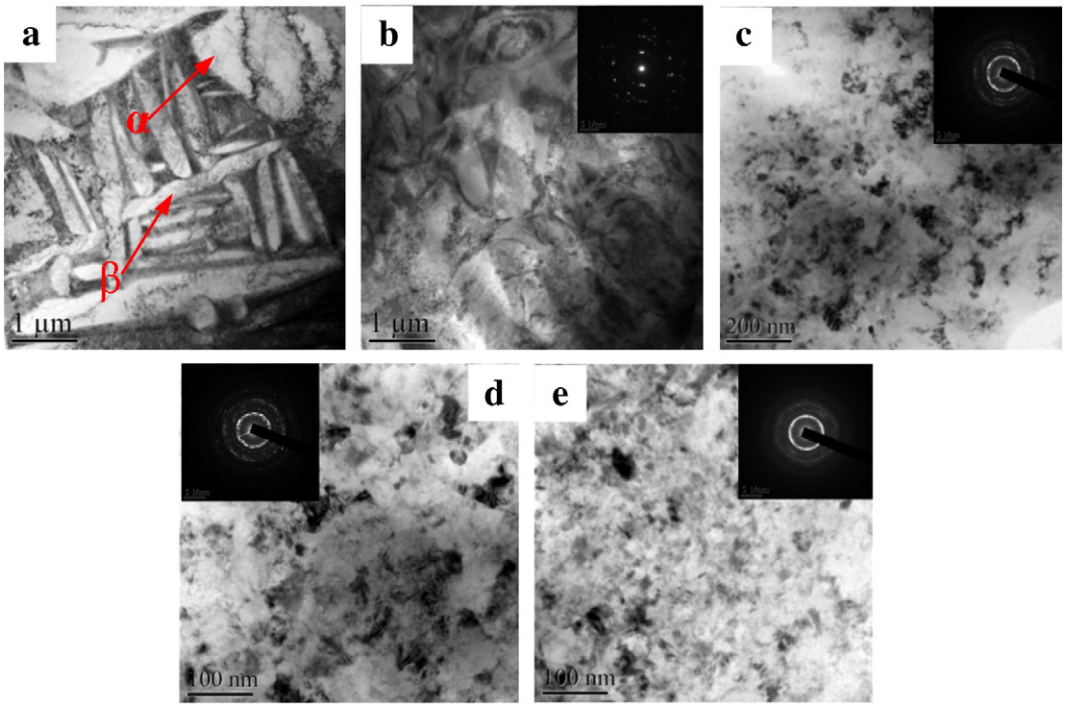

Fig. 4. TEM photographs and diffraction patterns of the surface layer of the titanium alloy samples with different LSP impacts. (a) Without LSP, (b) 1 impact, (c) 3 impacts, (d) 5 impacts and (e) 10 impacts.

On the section, because the kinetic energy is consumed and mainly transited to plastic energy with plastic deformation generated when the shock wave propagates into depth, the compressive residual stress decreases with the depth. The pressure of shock wave decreases with depth and less plastic deformation is generated. The plastically affected depth is about 600 μm for 1 impact, 1080 μm for 3 impacts, 1250 μm for 5 impacts and 1600 μm for 10 impacts. The four distribution curves demonstrate that more LSP impacts can increase plastically affected depth significantly, which is correlating well with the conclusions of Clauer et al. [38]. Due to the limited deformation in the material surface, the shock wave with higher pressure propagates into depth in the latter impacts. The shock wave induced by the latter impact can propagate into the deeper location and produce plastic deformation in the deeper depth. So increasing LSP impact is an effective way to improve the affected depth.

5. Microhardness distribution

Hardness is a basic mechanical property of the material, and it can be defined as the resistance to indentation. The hardness magnitude is the symbol of wear resistance for the material. Great hardness can bring in a good property of wear resistance and prevent the FOD to some extent. In this study, the Vickers microhardness of samples was tested by the MVS-1000JMT2 microhardness tester, using an indentation load of 500 g with a dwell time of 15 s at the section.

Fig. 6 shows the microhardness distribution curves on the section of TC11 titanium alloy samples with different LSP impacts. The original hardness is about 351 HV0.5. After LSP, the hardness has been effectively increased and the maximal hardness also locates at the material surface, similar to the distribution law of residual stress. The surface microhardness increases to 416 HV0.5 with only one LSP impact. With LSP impact

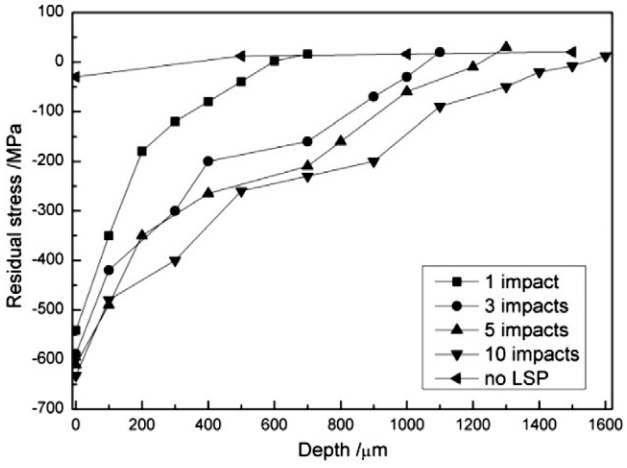

Fig. 5. Residual stress distribution on the cross section with different LSP impacts.

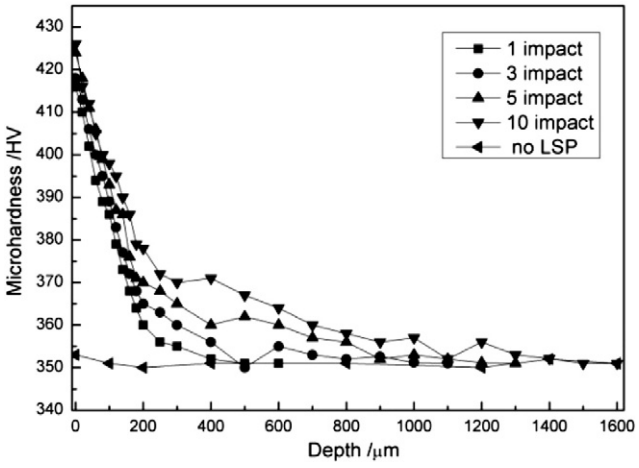

Fig. 6. Microhardness distribution on the cross-section with different LSP impacts.

increasing, the surface microhardness is 418 HV0.5, 424 HV0.5, and 426 HV0.5 respectively for 3 impacts, 5 impacts and 10 impacts. The surface microhardness increases with LSP impact, but the further improved amplitude is limit, only 2–3%. Work hardening and structural changes are the main factors of the hardness improvement. On the one hand, LSP has generated a severe plastic layer which leads to the cold working hardening. On the other hand, dislocations and nanocrystals which have been observed in the above TEM photographs (shown in Fig. 4) can improve the material hardness according to the dislocation strengthening theory and Hall–Petch formula. Thus limited plastic deformation restricts improving surface hardness with more LSP impacts further. However, the hardness-affected depth increases significantly with LSP impact. The affected depth of hardness is about 700 μm for one impact, 1100 μm for 3 impacts, 1300 μm for 5 impacts and 1500 μm for 10 impacts. It is also well consistent with the distribution rule of residual stress.

In depth, we can see that the hardness decreases with depth and there is a severe hardening layer, about 300 μm. In the severe hardening layer, the hardness decreases sharply. In contrast, the hardness decreases gradually below the severe hardening layer. The reason of hardness sharply decreasing in the severe hardening layer is the severe plastic deformation with refined grains which is resulted from the high amplitude pressure of shock wave. On the contrary, the hardness gradually decreasing in the deeper layer is ascribed to the dislocations, which is caused by the low amplitude pressure of attenuated shock wave. It is correlating with the previous conclusions about microstructure stratification after LSP [22] and hardness distribution on the section of TC17 titanium alloy [23].

6. Vibration fatigue

According to the technology standard (HB5277-84), thirty standard vibration fatigue specimens made of TC11 titanium alloy were designed by ourselves (shown in Fig. 7) and machined by Li-Ming Aero-Engine Co. The subsequent handling of specimens was as same as that of TC11 titanium alloy compressor blades.

Firstly the first-order mode and stress distribution of specimen in the vibration test were calculated by finite element analysis with the ABAQUS commercial software. The boundary condition is the blue shadow region fixed absolutely in Fig. 7. Fig. 8 is the first-order mode of the specimen and the resonant frequency is 315.6 Hz, close to the factual value, 316.8 Hz. The stress distribution of the specimen in the first-order vibration test is shown in Fig. 9. It illustrates that the maximal working stress locates at the notched part. The notched part is the weakness region of the specimen in vibration. So this region was confirmed to be the laser-peened region, as shown by the red dashed region in Fig. 7.

In order to avoid bending in one-sided LSP and improve the LSP process efficiency, the standard vibration specimens were treated by the two-sided LSP, in which two laser beams were shocked on the two sides of the specimen in simultaneous. The equipment structure of two-sided LSP is schematically shown in Fig. 10.

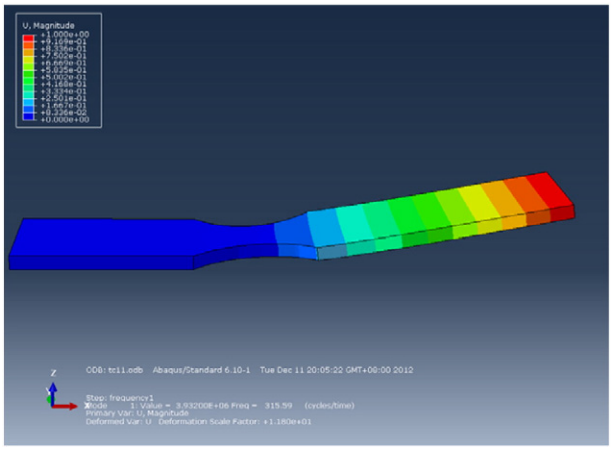

Fig. 8. The first-order mode of the vibration specimen. The greatest amplitude locates at the tip of the specimen.

According to the microstructure and mechanical properties of TC11 titanium alloy with different LSP impacts, three-impact is confirmed to be the most appropriate LSP impact. Firstly, the specimen surface integrity with three LSP impacts settles for the industry standard. The surface roughness (Ra) of the processed region is only 0.68 μm, lower than the standard (0.8 μm). However, it gets greater and can't fill the standard any more with 5/10 LSP impacts. Secondly the compressive residual stress and microhardness are improved to 589.2 MPa and 418 HV0.5 respectively with three LSP impacts. What is more, the nanostructure was generated, which was reported to be very useful for improving fatigue behavior, especially in elevated temperature [2,20,21]. Thirty specimens were tested in fatigue test, and one half of specimens were processed with three LSP impacts.

Fatigue tests were conducted at the maximum stress, room temperature and resonant frequency, in air, to measure the fatigue limit without and with LSP at 10^7 cycles. Vibration fatigue test was carried out on the D-300-3 electric vibration system, shown in Fig. 11. The tip amplitude of the standard vibration specimen was read from an optical microscope and monitored by an eddy current displacement sensor in the test. Gauges glued on the center of the notched region were used to demarcate the maximal vibration stress and monitor the strain in the vibration process. Once a fatigue crack develops in the specimen during the vibration test, the resonant frequency will shift. The test will be stopped when the resonant frequency decreased by 1%, usually prior to the crack propagating completely through the specimen.

According to the up-and-down fatigue method, the fatigue data were disposed into the fatigue up-and-down curve. The fatigue up-and-down curves without and with LSP are shown in Fig. 12. It can be calculated that the fatigue limit without LSP is 483.2 MPa. The fatigue limit of LSP processed specimens is improved to 593.6 MPa, about 22.8% increase. It indicates that LSP can improve the fatigue strength of TC11 titanium alloy effectively.

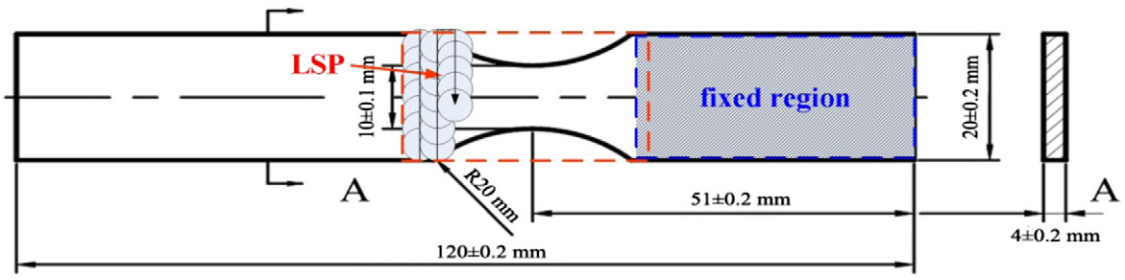

Fig. 7. Dimensions and LSP processed area of standard vibration components (the red dashed region is the LSP processed area and the blue shadow region is the fixed area in the vibration test).

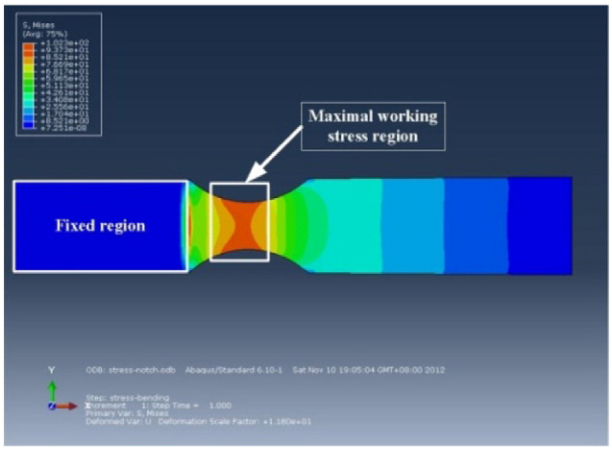

Fig. 9. Mises equivalent stress distribution in the first-order vibration condition.

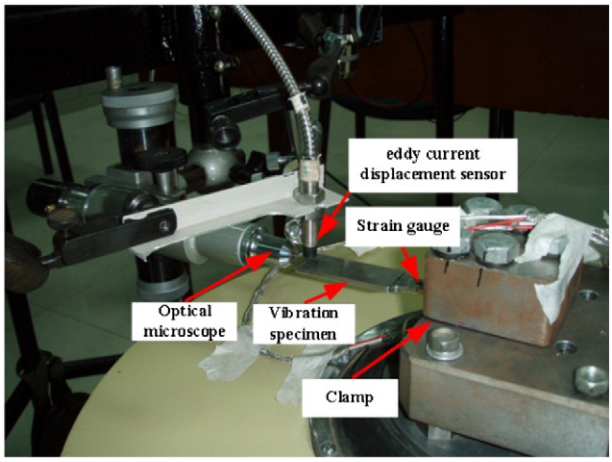

Fig. 11. State of a standard vibration specimen in the test process.

7. Fracture analysis and strengthening mechanism

7.1. Fracture analysis

After the fatigue test, vibration specimens were taken for fracture observation by the JEOL/JSM-6360LV scanning electron microscope. Fig. 13 is the typical fractography of specimens without and with LSP. According to the fractography, the fracture mechanism was analyzed. The effects of LSP on fatigue crack initiation and growth were discussed.

Comparing the fractography of specimens without and with LSP, some different features can be observed. Firstly the crack source of original specimens locates at the surface (shown in Fig. 13(a)), but the crack source locates in the subsurface after LSP, about 0.1 mm depth (shown in Fig. 13(b)). It may be ascribed to the positive action of high-amplitude compressive residual stresses and nanostructure at the surface. With the initiation of fatigue crack, the fracture can be divided into two parts, flat region and accidented region. The flat region is a symbol of fatigue crack extending slowly. Fig. 13(a) and (b) shows that the flat region with LSP is larger than that without LSP. It indicates that LSP can effectively reduce the FCGR. As shown in Fig. 13(c), many cleavage steps are generated in the flat region with LSP. The cleavage steps always result from dislocations and boundaries, which is the fracture characteristic of the complicated stress state. The phenomenon is caused by the compressive residual stress. The accidented region is a symbol of fatigue crack extending quickly. In Fig. 13(d), dense fatigue stripes and lots of secondary cracks are generated after LSP, which result from the blocking effect of residual stress, dislocations and new grain-boundaries. The appearance of dense fatigue stripes also illustrates that the FCGR reduces obviously. To sum up, residual stress and microstructural changes are both positive to delay the initiation of fatigue crack and reduce the FCGR in the HCF.

7.2. Discussion on strengthening mechanism

According to the above study on microstructure, mechanical properties and fatigue behavior, it indicates that the fatigue limit improvement of TC11 titanium alloy is mainly attributed to the comprehensive action of compressive residual stresses and structural changes induced by LSP. The strengthening mechanism can be concluded as following:

(I) In the fatigue crack initiation stage, the residual compressive stress plays an important role. According to the Goodman theory [39], the compressive residual stress can counteract a part of work tensile stress and the fatigue strength will be improved. Compressive residual stress enhances the fatigue limit of the strengthened layer and compels fatigue cracks to initiate at the vulnerable area, where working stress is much smaller than that at the surface and there are more restrictions for deformation. In other words, it is hard for crack initiating there. Thus, compressive residual stress dramatically prolongs the fatigue crack initiation life.

At the same time, few crystal defects remain in the nanocrystals (shown in Fig. 4) of the nanostructure layer. And grain refinement brings in the improvement of material strength according to Hall–Petch formula. So the condition of crack initiation is difficult to reach.

(II) In the growth stage of fatigue crack, residual compressive stress can improve the threshold of crack growth [9]. Once the fatigue crack initiates, the decreasing stress intensity factor range ΔK and stress ratio R caused by compressive residual stress can reduce fatigue crack growth rate [40]. Meanwhile, compressive residual stress greatly increases the closing force of microscopic cracks; thereby, it retards their propagation. What is more, some cracks are compelled to swerve or stopped to extend, so many secondary-cracks were generated in the accidented region in Fig. 13(d).

Besides the positive contribution of compressive residual stress for fatigue crack growth, the structural changes also play an important role. Refined grains bring in more grain boundaries which can improve

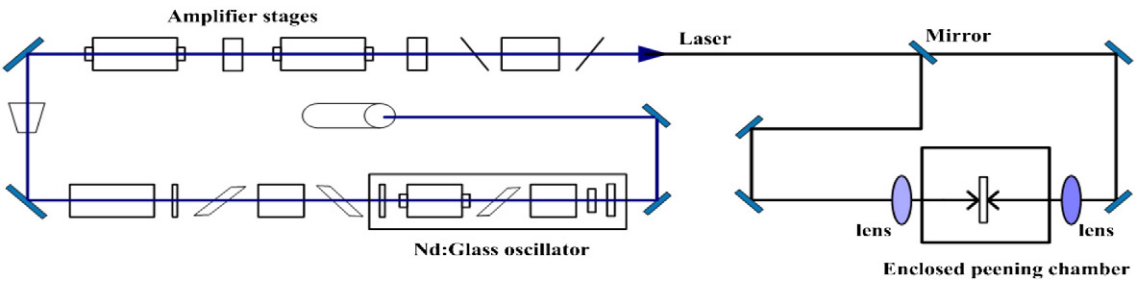

Fig. 10. Schematic structure of the two-sided laser shock peening. The laser pulse sent from the laser is divided into two pulses via the optical mirror and lenses which strike on the target at the same time.

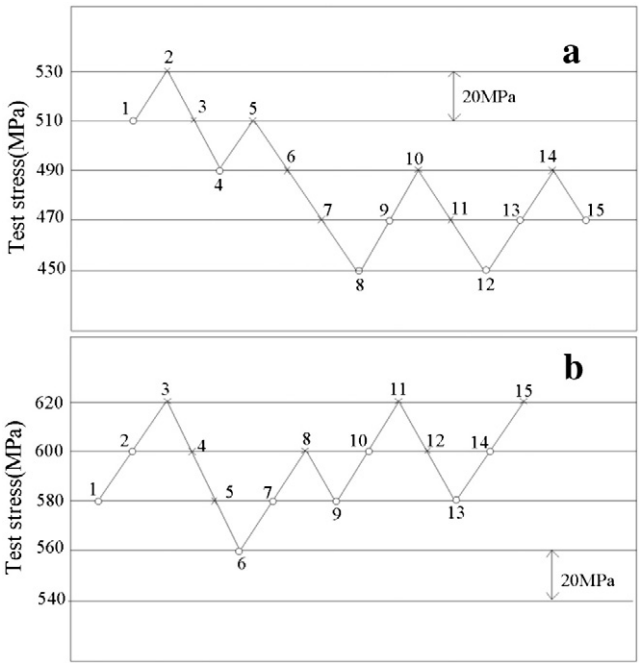

Fig. 12. Fatigue up-and-down curves of TC11 titanium alloy specimens. (a) Without LSP and (b) with LSP.

the resistance for slip deformation, restrain the generation of slip bands and increase the grain boundary resistance for crack growth. When fatigue crack initiated, the crack growth rate will be decreased under the blocking of the tremendous grain boundaries. In the subsurface, high density dislocations in grains can restrain the plastic flow and block the crack growth.

In addition, compressive residual stress can be relaxed under the cycle loading [41]. So the structural changes are the main strengthening factor for HCF performance when residual stress relaxed in the later fatigue test.

8. Conclusions

(1) High density dislocations are generated in the surface layer of the TC11 titanium alloy sample with only one LSP impact. Under three LSP impacts, the grains are refined and nanocrystals are generated. The refinement degree will be basically saturated when the LSP impact is greater than 5, but the grain orientation becomes random and uniform.

(2) Compressive residual stress and microhardness at the surface both increases with LSP impact, but limited. However, the affected depth can be effectively increased with LSP impact.

(3) The fatigue limit of standard vibration specimens with three LSP impacts is improved from 483.2 MPa to 593.6 MPa, about 22.8% increase. Via the fracture analysis, the crack source locates in the subsurface and the flat region is enlarged after LSP. In the accidented region, more secondary-cracks are generated and the fatigue stripes become denser.

(4) Compressive residual stress and nanostructure with few crystal defects lead to the fatigue crack hard to be initiated at the surface. So the initiation is retarded and the fatigue crack initiation life is prolonged. On the other hand, the decreasing of stress intensity factor range and stress ratio caused by LSP can reduce the FCGR. Moreover, more grain boundaries and high density dislocations can block the fatigue crack growth. However, structural changes are the main strengthening factor for HCF performance when residual stress relaxed in the later fatigue test.

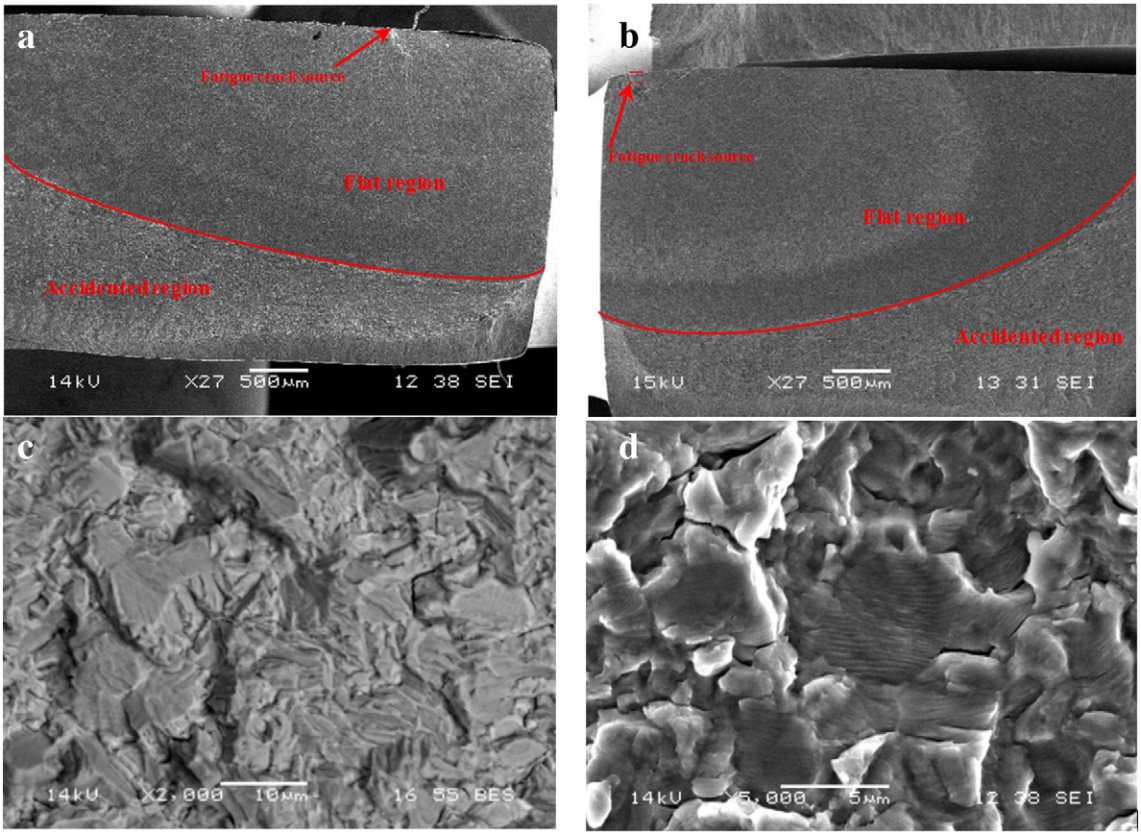

Fig. 13. Typical fractography of specimens after fatigue test. (a) Macroscopic fractography without LSP, (b) macroscopic fractography with LSP, (c) enlarged view of the flat region with LSP and (d) enlarged view of the accidented region with LSP.

Acknowledgments

The authors are very grateful to professor Lu of Xi'an University of technology and professor Shi of Xidian University for their useful comments and suggestions on the microstructural observations and fracture analysis. Financial support for this study was provided by the National Science Foundation of China (51205406).

References

[1] G.H. Majzoobia, K. Azadikhahb, J. Nematia, Mater. Sci. Eng. A 516 (2009) 235–247.
[2] R.K. Nalla, I. Altenberger, U. Noster, G.Y. Liu, B. Scholtes, R.O. Ritchie, Mater. Sci. Eng. A 355 (2003) 216–230.
[3] K.L. Kevin, R.H. Michael, Tribol. Int. 42 (2009) 1250–1262.
[4] C.S. Montross, T. Wei, L. Ye, G. Clark, Y.W. Mai, Int. J. Fatigue 24 (2002) 1021–1036.
[5] P. Peyre, R. Fabbro, P. Merrien, H.P. Lieurade, Mater. Sci. Eng. A 210 (1996) 102–113.
[6] C. Ye, S. Suslov, B.J. Kim, E.A. Stach, G.J. Cheng, Acta Mater. 59 (2011) 1014–1025.
[7] K. Masaki, Y. Ochi, T. Matsumura, Y. Sano, Mater. Sci. Eng. A 468–470 (2007) 171–175.
[8] H. Lim, P. Kim, H. Jeong, S. Jeong, J. Mater. Process. Technol. 212 (2012) 1347–1354.
[9] W. Sagawaa, T. Aokib, T. Itoua, K. Enomotoc, E. Hayashid, T. Ishikawae, Nucl. Eng. Des. 239 (2009) 655–664.
[10] M. Barletta, G. Rubino, A. Gisario, Wear 271 (2011) 2016–2024.
[11] Y. Sano, M. Obata, T. Kubo, N. Mukai, M. Yoda, K. Maski, Y. Ochi, Mater. Sci. Eng. A 417 (2006) 334–340.
[12] O. Hatamleh, J. Lyons, R. Forman, Int. J. Fatigue 29 (2007) 421–434.
[13] S. Spanrad, J. Tong, Mater. Sci. Eng. A 528 (2011) 2128–2136.
[14] I. Watanabe, M. Mcbride, P. Newton, K.S. Kurtz, Dent. Mater. 25 (2009) 629–633.
[15] C. Cellard, D. Retraint, M. Francois, E. Rouhaud, D.L. Saunier, Mater. Sci. Eng. A 532 (2012) 362–372.
[16] J.J. Ruschau, R. John, S.R. Thompson, T. Nicholas, J. Eng. Mater. Technol. ASME 121 (1999) 321–329.
[17] J.J. Ruschau, R. John, S. Thompson, T. Nicholas, Int. J. Fatigue 21 (1999) S199–S209.
[18] X.C. Zhang, Y.K. Zhang, J.Z. Lu, F.Z. Xuan, Z.D. Wang, S.T. Tu, Mater. Sci. Eng. A 527 (2010) 3411–3415.
[19] E. Maawad, Y. Sano, L. Wagner, H.G. Brokmeier, Ch. Genzel, Mater. Sci. Eng. A 536 (2012) 82–91.
[20] I. Nikitin, I. Altenberger, Mater. Sci. Eng. A 465 (2007) 176–182.
[21] I. Altenberger, R.K. Nalla, Y. Sano, L. Wagner, R.O. Ritchie, Int. J. Fatigue 44 (2012) 292–302.
[22] L.C. Zhou, Y.H. Li, W.F. He, G.Y. He, X.F. Nie, D.L. Chen, Z.L. Lai, Z.B. An, Mater. Sci. Eng. A 578 (2013) 181–186.
[23] X.F. Nie, W.F. He, Q.P. Li, N.D. Long, Y. Chai, J. Laser Appl. 25 (2013) 042001-1–042001-6.
[24] Aeronautical Manufacture Engineering Committee, Aeronautical manufacture engineering handbook, Aerospace Industry Press, Beijing, 1997.
[25] X.F. Nie, N.D. Long, W.F. He, Q.P. Li, Mater. Sci. Forum 694 (2011) 946–950.
[26] K. Lu, J. Lu, J. Mater. Sci. Technol. 15 (1999) 193–197.
[27] T.S. Wang, J.K. Yu, B.F. Dong, Surf. Coat. Technol. 200 (2006) 4777–4781.
[28] G. Liu, J. Lu, K. Lu, Mater. Sci. Eng. A 286 (2000) 91–95.
[29] K. Lu, J. Lu, Mater. Sci. Eng. A 375 (2004) 38–45.
[30] N.R. Tao, Z.B. Wang, W.P. Tong, M.L. Sui, J. Lu, K. Lu, Acta Mater. 50 (2002) 4603–4616.
[31] J.Z. Lu, K.Y. Luo, Y.K. Zhang, C.Y. Cui, G.F. Sun, J.Z. Zhou, L. Zhang, J. You, K.M. Chen, J. W. Zhong, Acta Mater. 58 (2010) 3984–3994.
[32] J.Z. Lu, K.Y. Luo, Y.K. Zhang, G.F. Sun, Y.Y. Gu, J.Z. Zhou, X.D. Ren, X.C. Zhang, L.F. Zhang, K.M. Chen, C.Y. Cui, Y.F. Jiang, A.X. Feng, L. Zhang, Acta Mater. 16 (2010) 5354–5362.
[33] M.A. Meyers, F. Gregori, B.K. Kad, M.S. Schneider, D.H. Kalantar, B.A. Remington, G. Ravichandran, T. Boehly, J.S. Wark, Acta Mater. 51 (2003) 1211–1228.
[34] M.A. Meyers, G. Subhash, B.K. Kad, L. Prasad, Mech. Mater. 17 (1994) 175.
[35] A.H. Clauer, B.P. Fairand, B.A. Wilcox, Metal. Trans. A 8 (1976) 1871–1876.
[36] Y.K. Zhang, C. Yu, Mater. Sci. Eng. A 257 (1998) 322–327.
[37] P. Peyer, L. Berthe, X. Scherpareel, R. Fabbro, Mater. Sci. 33 (1998) 1421–1429.
[38] A.H. Clauer, Mater. Soc. AIME (1996) 217–230.
[39] E. I. Haddad M.H., K.J. Topper, L.P. Pook. London: Oxford University Press. 1974.
[40] D. Schnubela, M. Horstmanna, V. Ventzkea, S. Riekehra, P. Staron, T. Fischer, N. Huber, Mater. Sci. Eng. A 546 (2012) 8–14.
[41] Yuji Sano, Koichi Akita, Kazuya, Rie Sumiya, Toshiyuki Saito, Chihiro Narazaki, Int. J. Struct. Integr. 2 (2011) 42–50.